Description and characterization of plasmonic Gaussian beams

2017 J. Opt. 19 085001

(http://iopscience.iop.org/2040-8986/19/8/085001)

IOP Publishing Journal of Optics
J. Opt. 19 (2017) 085001 (5pp) https://doi.org/10.1088/2040-8986/aa7724

Description and characterization of plasmonic Gaussian beams

Cesar E Garcia-Ortiz[1], Eduardo Pisano[2] and Victor Coello[2]

[1] CONACYT—CICESE, Unidad Monterrey, Alianza Centro 504, PIIT Apodaca, 66629, Mexico
[2] CICESE, Unidad Monterrey, Alianza Centro 504, Apodaca, NL 66629, Mexico

E-mail: cegarcia@cicese.mx

Received 24 March 2017, revised 12 May 2017
Accepted for publication 5 June 2017
Published 14 July 2017

Abstract

In this work, we present for the first time a detailed description and experimental characterization of plasmonic Gaussian beams (PGBs), as well as the analytical expression to describe their field and intensity distributions. The propagation parameters of the PGBs, such as the divergence angle, Rayleigh range, beam width function, and the beam waist are determined experimentally in accordance to the proposed model. The radius of curvature of the wavefront and the Gouy phase shift of PGBs can also be predicted using this method.

Keywords: Gaussian beams, plasmonics, diffraction

(Some figures may appear in colour only in the online journal)

1. Introduction

Plasmonics is a branch of nano-optics which deals with the excitation and manipulation of surface plasmon polaritons (SPPs) [1]. Single metallic ridges can couple free-propagating light of a broad range of wavelengths (in the plasmonic range) into SPPs by illuminating with a focused Gaussian beam. This excitation technique was first introduced and characterized in 2003 as an efficient and local alternative to couple light into SPPs, which generates an SPP beam propagating perpendicular to the ridge structure [2]. Since then, the method has been widely used as a standard SPP excitation mechanism [3–7], but less attention has been directed to the description and characteristics of the beam.

Generation and characterization of different types of plasmonic beams have gained the attention of different research groups in the last decade. Self-accelerating, and quasi diffraction-free beams, such as the Airy [8, 9] and the Bessel beam [10], have been studied analytically and characterized experimentally. In this direction, we aim for the study and characterization of the propagation parameters of plasmonic beams excited as mentioned above. It was already observed that if SPPs are excited with a transverse-electromagnetic (TEM_{00}) Gaussian beam, the divergence of the generated SPP must equal the divergence of the excitation light [11]. This fact served as a motivation for the present work and lead us to study the properties and parameters transferred from the Gaussian beam to the SPP. Our hypothesis is that the generated SPP beam inherits not only the divergence of the source, but all of the well-known Gaussian properties, such as the Rayleigh range, beam width function, intensity distribution, radius of curvature of the wavefront, and the Gouy phase shift [12]. Henceforth, SPP beams generated in the aforementioned configuration will be referred to as plasmonic Gaussian beams (PGBs) along the text.

In this work, we find the expressions that describe the field and intensity distribution of PGBs as solutions of the paraxial wave equation. Next, we characterize experimentally the PGBs with leakage-radiation microscopy (LRM), using microscope objectives for excitation with three different numerical apertures (NA = 0.10, 0.25, and 0.40).

2. Analytical description

Gaussian beams are solutions to the paraxial wave equation [12], and the two-dimensional (2D) expression of the field

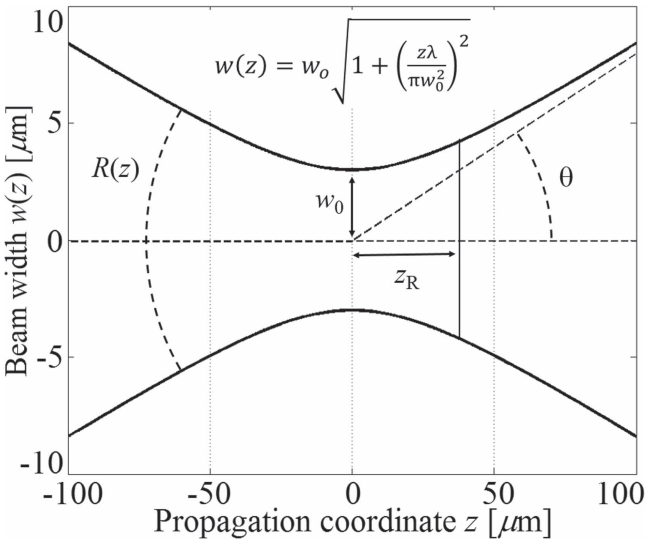

Figure 1. Beam width of a Gaussian beam as a function of the propagation coordinate z. The beam waist w_0, Rayleigh range z_R, divergence angle θ and the radius of curvature $R(z)$ are depicted in the graph. This example is obtained using $w_0 = 3.5$ μm and $\lambda_0 = 740$ nm. The axes are scaled for clarity.

propagating in the z-direction can be expressed as

$$\psi_G(x, z) = \psi_0\sqrt{\frac{w_0}{w(z)}}\exp\left(\frac{-x^2}{w(z)^2}\right) \times \exp\left[-i\left(k_0 z + k_0\frac{x^2}{2R(z)} - \varphi(z)\right)\right], \quad (1)$$

where $w(z)$, commonly known as the beam width or radius, is the radial distance from the propagation axis of the beam at which the field amplitude has decayed $1/e$ times (or $1/e^2$ of the intensity), and ψ_0 is the field amplitude in the origin. The beam waist $w_0 = w(0)$ corresponds to the minimal value of $w(z)$, and x is the transverse coordinate. Here, $k_0 = 2\pi/\lambda_0$ corresponds to the free-space wavevector, and $R(z)$ and $\varphi(z)$ are the radius of curvature of the wavefront and the 2D Gouy phase shift, respectively. The beam width is a function of the propagation coordinate, and can be expressed as

$$w(z) = w_0\sqrt{1+\left(\frac{z\lambda M^2}{\pi w_0^2}\right)^2}. \quad (2)$$

In practice, the beams generated in laser systems may vary on how well they approximate to a Gaussian TEM_{00} mode (figure 1). In this context, the factor M^2 is introduced in equation (2) to account for the beam quality. The M^2 factor corresponds to the ratio of the beam parameter products (BPP) (i.e. the product of the beam waist and the far-field beam divergence) of the real case divided by the ideal case $M^2 = w_{0,real}\theta_{real}/w_{0,ideal}\theta_{ideal}$. The ideal case corresponds to $M^2 = 1$, and $w_0 = w_{0,ideal}$ is diffraction limited. For the real case ($M^2 > 1$), the beam waist is wider and determined by the BPP. Gaussian beams are also characterized by the Rayleigh range $z_R = \pi w_0^2/\lambda M^2$, defined as the distance along z where the beam width is $\sqrt{2}$ larger than w_0, the divergence angle $\theta \approx \lambda M^2/\pi w_0$, that corresponds to the radial angle at which the beam spreads asymptotically, the 2D Gouy phase shift $\varphi(z) = ½ \text{ atan}(z/z_R)$, and the radius of curvature of the wavefront

$$R(z) = z\left[1+\left(\frac{\pi w_0^2}{z\lambda M^2}\right)^2\right]. \quad (3)$$

In the case of a 2D Gaussian beam, the intensity distribution can be expressed as

$$I(x, z) = I_0\left(\frac{w_0}{w(z)}\right)\exp\left(\frac{-2x^2}{w(z)^2}\right), \quad (4)$$

where the second factor describes the intensity decay along the propagation coordinate caused by the divergence of the beam (diffraction), and the exponential term corresponds to the Gaussian transverse distribution.

So far, we have outlined the most representative parameters and expressions that describe the propagation of real (non-ideal) Gaussian beams, and special attention was directed to the 2D case (cylindrical wave). Now, we focus on the expressions the SPP beam. The field of a plane SPP wave, invariant in the x-coordinate, propagating in the z-direction along a metal–insulator interface can be defined as

$$\psi_{SPP}(y, z) = \psi_0\exp\left[i(\beta z + ik_y y)\right], \quad (5)$$

where the y-coordinate corresponds to the direction perpendicular to the interface, $\beta = \beta' + i\beta''$ is the complex propagation constant, and k_y is the out-of-plane evanescent wavevector. The intensity distribution of the plane SPP wave reads simply as

$$I(y, z) = I_0\exp\left(\frac{-z}{L_{SP}}\right)\exp(-2k_y y), \quad (6)$$

where $L_{SP} = 1/(2\beta'')$ is known as the propagation length of the SPP, and is defined as the distance along the propagation where the intensity has decreased by a factor of $1/e$. Combining equations (1) and (5), we can define the field of a PGB as

$$\psi_{PGB}(x, y, z) = \psi_0\sqrt{\frac{w_0}{w(z)}}\exp\left(\frac{-x^2}{w(z)^2}\right) \times \exp\left[i\left(\beta z + ik_y y - \beta\frac{x^2}{2R(z)} + \varphi(z)\right)\right], \quad (7)$$

which also satisfies the paraxial wave equation, since the evanescent term $\exp(-k_y y)$ is independent of the transverse and propagation coordinates (x, z). Using this result, the intensity distribution is determined by

$$I(x, y, z) = I_0\left(\frac{w_0}{w(z)}\right)\exp\left(\frac{-z}{L_{SP}}\right)\exp(-2k_y y) \times \exp\left(\frac{-2x^2}{w(z)^2}\right). \quad (8)$$

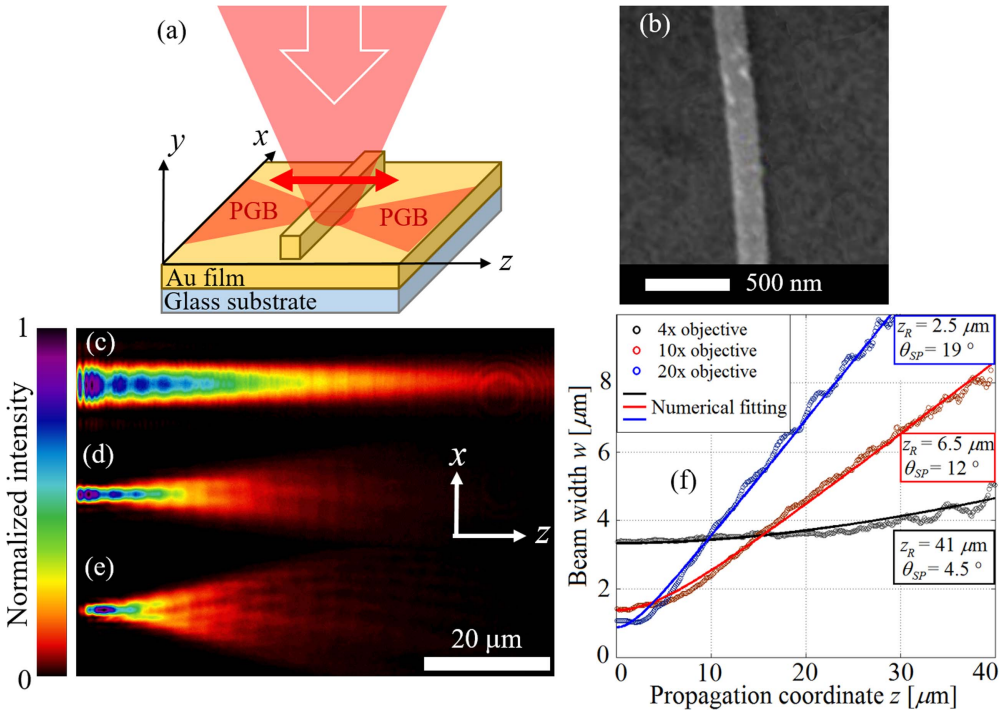

Figure 2. (a) Schematic of the setup used to excite the PGBs. The double arrow indicates the polarization of the incident light. (b) Scanning electron microscopy image of the gold ridge. (c)–(e) LRM images (image plane) of the intensity distribution of PGBs, propagating from left to right, focused with the (c) 4×, (d) 10×, and (e) 20× objectives. (f) Measured beam width of the PGBs as a function of the propagation coordinate z. The solid lines correspond to the numerical fitting of the semi-analytical expression for the beam width.

Table 1. Parameters of the focusing objectives and of the corresponding generated PGBs.

Microscope objectives				PGBs			
Magnification	NA	Acceptance angle θ_a (°)	Minimum waist w_m (μm)	θ_{SP} (°)	w_0 (μm)	z_R (μm)	M^2 (fit)
4×	0.10	5.7	2.39	4.5	3.30	41	1.15
10×	0.25	14	0.97	12	1.37	6.5	1.26
20×	0.40	23	0.59	19	0.87	2.5	1.29

3. Experimental characterization

The experiment consists of generating PGBs by focusing the laser beam with a microscope objective onto a gold ridge sitting on top of a gold thin-film. The gold ridges (200 nm wide and 70 nm thick) were patterned on top of a 70 nm thick gold film using e-beam lithography (figure 2(a)). The laser was operated at a wavelength of 740 nm, linearly polarized (perpendicular to the ridges), and with a near TEM_{00} fundamental Gaussian beam (measured beam quality factor $M_L^2 = 1.01 \pm 0.03$). The beam quality factor of the laser was estimated by measuring the beam width at different positions near the focus of a lens, and a CCD camera to record the beam width size.

The scattered light generates two symmetrical PGBs propagating in the perpendicular direction to the ridge. Both beams have almost identical properties, and only one of them is used for this study. To generate PGBs with different properties, three different focusing objectives were used in the experiment, since the associated divergence angle is determined by the numerical aperture of the microscope objective. A beam expander situated before the focusing objective is used to cover the complete area of the objective rear aperture, so that the divergence of the beam fits the acceptance angle $\theta_a = \text{asin(NA)}$ of the objective. Table 1 synthesizes the parameters of the focused beam after each objective, including the minimum radius of the beam waist in the focal plane, if the whole rear aperture is illuminated, given by $w_m = M_L^2 \lambda_0 / \theta\pi$.

The intensity distribution of the generated PGBs are obtained from the LRM images (figures 2(c)–(e)). The experimental setup and a detailed description of the principle of operation of LRM can be found in the [11, 13]. For each of the beams, the beam width w was measured as a function of the position in the propagation direction, using a Gaussian fit along the transverse direction x. The obtained data points describe the divergence of the beam, and are used to find w_0 and the M^2 factor through numerical fitting using equation (2) (figure 2(f)). It must be noted that the value used for λ is $\lambda_{SP} = 2\pi/\beta' = 719$ nm, i.e. the wavelength of an SPP in a gold–air interface excited with a free-space wavelength of 740 nm. In

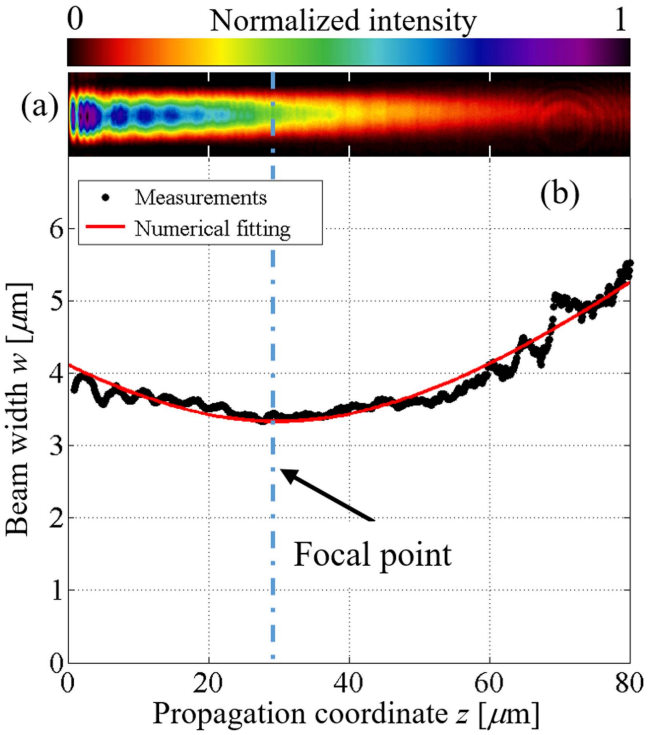

Figure 3. (a) LRM image of the intensity distribution of the PGB generated with the 4× objective and (b) the measured beam width starting from the position of the ridge. The dashed line indicated the position of the beam waist (focal point), which is not perceptible in (a). The scale in (a) is the same as in (b).

most cases, it is not possible to determine the precise position of the PGB waist (focal point) by naked eye observation of the LRM images. In this sense, the fitted curve also allows to find the position of the focal point, if z is replaced by $(z + \delta z)$ and leave δz as a new fitting parameter (figure 3). Using the obtained values of w_0 and M^2, is now possible to estimate the values of the Rayleigh range, divergence and the radius of curvature of the wavefront along the propagation direction. Table 1 shows these results, which can be compared to the parameters of the focusing objectives. As expected, the divergence angle of the PGB approximately matches the acceptance angle of the objective, but with an angle reduction of 14%–21%. The decrease of divergence is compensated with a higher PGB beam waist, with an increase of 37%–47%. This tradeoff can be better understood if we introduce the relation $M^2 = w_0\theta_{SP}/w_m\theta$, which we can define as the PGB beam quality factor. Since the laser has an $M^2 \sim 1$, we can consider the BPP $= w_m\theta$ as close to ideal. In this regard, we can estimate the value of the PGB M^2 factor by solving the relation, if w_0 and θ_{SP} are known. The results are similar to the obtained with numerical fitting, giving values of 1.09, 1.21, and 1.22, for the 4×, 10×, and 20×, respectively. It is important to note that in this case, the excitation beam and generated PGBs have different wavelengths, thus this approach, although very similar, is not the exact same as for embedded Gaussian beams. The radius of curvature of the wavefront of each PGB can be predicted and estimated from equation (3) using the parameters obtained experimentally (figure 4(a)). It is of special interest to see that the PGB generated with the 4× objective, has a quasi-plane-wave behavior below 5 μm, making it suitable for experiments were a plane wavefront is preferred. The objectives with higher magnification reach much lower values of R, close to the excitation point, and changes rapidly in short distances. The Gouy phase shift was also estimated and shows that the phase shift can be appreciated at this scale (figure 4(b)). It is observed that a phase shift of almost $3\pi/8$ occurs within the first 5 μm, in the case of the 20× objective. For the PGB generated with the 4× objective, the phase shift changes more slowly and barely surpasses a shift of $\pi/4$ after 50 μm. This considerations can be very important when designing specific experiments where a precise knowledge of the phase and wavefront shape is required at every point, or in numerical simulations of plasmonic beams. For example, when using PGBs in interferometric plasmonic devices, abrupt changes in the phase can have different outputs or responses.

The divergence of a PGB can hinder the estimation of the propagation length. To recover the correct value, our description can be used to determine L_{SP} accurately. Equation (8) describes the intensity distribution of the PGB, as well as the propagation losses and divergence. To prove the validity of the method, we take intensity profiles along the propagation coordinate z, at the axis point ($x = 0$). Mapping the intensity through the axis avoids the problem of using a more complex coordinate system (hyperbolic coordinate), and also the last term in equation (8) becomes unity. The intensity profiles are processed with numerical fitting, using the parameters obtained before. L_{SP} is left as the only fitting parameter. The results show that, despite the strong decay in the intensity due to divergence, it is still possible to recover the information which corresponds to the propagation losses (figure 4(c)). The obtained values were $L_{SP}(4\times) = 32 \pm 2$ μm, $L_{SP}(10\times) = 32 \pm 3$ μm, $L_{SP}(20\times) = 28 \pm 3$ μm. Evidently, the value of L_{SP} must be the same for all the PGBs, since it is only dependent on the medium where it propagates and the excitation wavelength. The results are in good agreement with our hypothesis, with minor deviations due to experimental noise.

4. Conclusions

In conclusion, we have presented a detailed description and characterization of PGBs, generated by exciting SPPs using microscope objectives with different NA. We have presented an analytical expression which describes the field and intensity distributions of PGBs, introducing the M^2 parameter to characterize the quality of the beam. All the parameters that govern the propagation of the PGB, such as the divergence angle, Rayleigh range, beam width and waist were characterized experimentally, as well as an M^2 factor for each of the beams. Moreover, this approach allowed for an accurate estimation of the propagation losses, even for diverging plasmonic beams. The radius of curvature of the wavefront and the Gouy phase shift were estimated from the experimental values and the proposed model. A direct measurement of these last two parameters can be

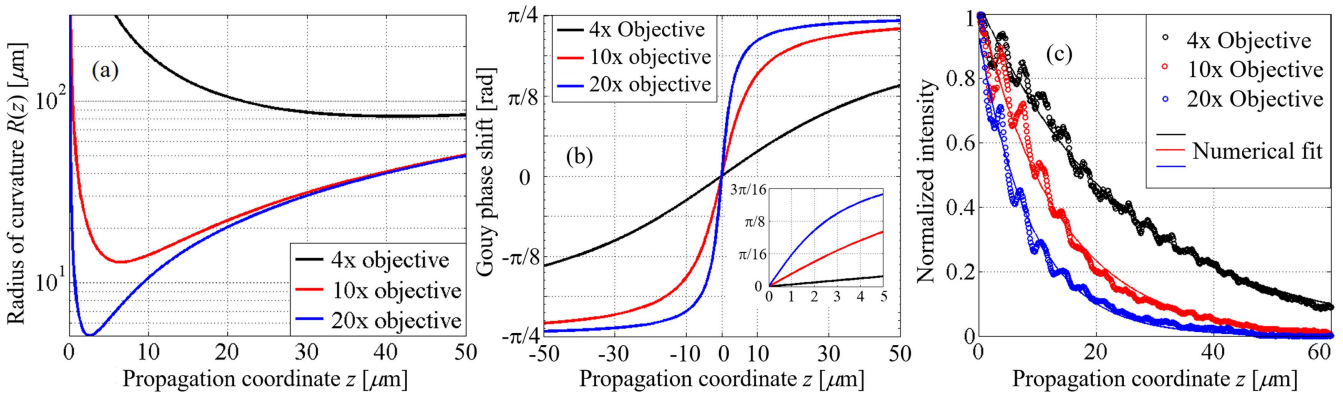

Figure 4. (a) Radius of curvature of the wavefront and (b) Gouy phase shift as a function of the propagation coordinate for the three PGBs excited with the different focusing objectives. The inset in (b) shows a zoom of the central area. (c) Intensity profiles along the axis $x = 0$, in the propagation direction showing the intensity decay due to propagation losses and divergence.

obtained via near-field imaging with phase detection. Such experiments could, in principle, be performed with a modified scanning near-field optical microscope with phase detection, such as the one used in [14, 15].

Acknowledgments

We acknowledge the financial support from CONACYT Basic Scientific Research Grant No. 250719 and No. 252621. We thank the help of Dr Rodolfo Cortes (GNO Mexico) for insightful discussions.

Note added in proof. When completing our work, we found that the Gouy phase shift of PGBs has been measured and reported using LRM with phase detection [16].

References

[1] Maier S 2007 *Plasmonics: Fundamentals and Applications* (Berlin: Springer)
[2] Ditlbacher H, Krenn J R, Hohenau A, Leitner A and Aussenegg F R 2003 Efficiency of local light-plasmon coupling *Appl. Phys. Lett.* **83** 3665
[3] Ditlbacher H, Krenn J R, Felidj N, Lamprecht B, Schider G, Salerno M, Leitner A and Aussenegg F R 2002 Fluorescence imaging of surface plasmon fields *Appl. Phys. Lett.* **80** 404
[4] Wang B and Lalanne P 2010 Surface plasmon polaritons locally excited on the ridges of metallic gratings *J. Opt. Soc. Am.* A **27** 1432
[5] Radko I P, Bozhevolnyi S I, Brucoli G, Martín-Moreno L, García-Vidal F J and Boltasseva A 2009 Efficient unidirectional ridge excitation of surface plasmons *Opt. Express* **17** 7228
[6] Radko I P, Bozhevolnyi S I, Brucoli G, Martín-Moreno L, García-Vidal F J and Boltasseva A 2008 Efficiency of local surface plasmon polariton excitation on ridges *Phys. Rev.* B **78** 115115
[7] Pisano E, Coello V, Garcia-Ortiz C E, Chen Y, Beermann J and Bozhevolnyi S I 2016 Plasmonic channel waveguides in random arrays of metallic nanoparticles *Opt. Express* **24** 17080
[8] Li L, Li T, Wang S M, Zhang C and Zhu S N 2011 Plasmonic Airy beam generated by in-plane diffraction *Phys. Rev. Lett.* **107** 126804
[9] Zhang P, Wang S, Liu Y, Yin X, Lu C, Chen Z and Zhang X 2011 Plasmonic Airy beams with dynamically controlled trajectories *Opt. Lett.* **36** 3191
[10] Garcia-Ortiz C E, Coello V, Han Z and Bozhevolnyi S I 2013 Generation of diffraction-free plasmonic beams with one-dimensional Bessel profiles *Opt. Lett.* **38** 905
[11] Drezet A, Hohenau A, Koller D, Stepanov A, Ditlbacher H, Steinberger B, Aussenegg F R, Leitner A and Krenn J R 2008 Leakage radiation microscopy of surface plasmon polaritons *Mater. Sci. Eng.* B **149** 220
[12] Goldsmith P F 1997 *Quasioptical Systems: Gaussian Beam Quasioptical Propagation and Applications* (New York: Wiley-IEEE)
[13] Garcia C, Coello V, Han Z, Radko I P and Bozhevolnyi S I 2012 Partial loss compensation in dielectric-loaded plasmonic waveguides at near infra-red wavelengths *Opt. Express* **20** 7771
[14] Zenin V A, Andryieuski A, Malureanu R, Radko I P, Volkov V S, Gramotnev D K, Lavrinenko A V and Bozhevolnyi S I 2015 Boosting local field enhancement by on-chip nanofocusing and impedance-matched plasmonic antennas *Nano Lett.* **15** 8148
[15] Andryieuski A, Zenin V A, Malureanu R, Volkov V S, Bozhevolnyi S I and Lavrinenko A V 2014 Direct characterization of plasmonic slot waveguides and nanocouplers *Nano Lett.* **14** 3925
[16] Birr T, Fischer T, Evlyukhin A B, Zywietz U, Chichkov B N and Reinhardt C 2017 Phase-resolved observation of the gouy phase shift of surface plasmon polaritons *ACS Photonics* **4** 905–8